atmosphere

MDPI

Article

Topographic Algebraic Rossby Solitary Waves: A Study Using Physics-Informed Neural Networks

Weiqi Zhang, Quansheng Liu, Liqing Yue and Ruigang Zhang *

School of Mathematical Sciences, Inner Mongolia University, Hohhot 010030, China; 32336071@mail.imu.edu.cn (W.Z.); smslqs@imu.edu.cn (Q.L.); judy_yue@imu.edu.cn (L.Y.)
* Correspondence: rgzhang@imu.edu.cn

Abstract

This study explores the influence of topography on Rossby solitary waves by analyzing the dynamics in both inner and outer regions, with solutions matched at the boundary. Using perturbation methods, the Benjamin–Davis–Ono (BDO) equation is derived from the shallow-water equations to characterize the amplitude evolution of Rossby algebraic solitary waves. The Physics-Informed Neural Networks (PINNs) method is applied to numerically solve the BDO equation, effectively capturing its nonlinear behavior and simulating the propagation of Rossby algebraic solitary waves under diverse topographic and external conditions. The results demonstrate that variations in key parameters significantly alter topographic effects, thereby impacting the amplitude of solitary waves. These findings provide valuable insights into the potential consequences of global warming and other external disturbances on the behavior of Rossby waves.

Keywords: Rossby algebraic solitary waves; Benjamin-Davis-Ono equation; Physics-Informed Neural Networks; shallow-water model equations; nonlinear propagation

check for updates

Academic Editor: Eugene Rozanov

Received: 6 October 2025
Revised: 10 November 2025
Accepted: 13 November 2025
Published: 17 November 2025

Citation: Zhang, W.; Liu, Q.; Yue, L.; Zhang, R. Topographic Algebraic Rossby Solitary Waves: A Study Using Physics-Informed Neural Networks. *Atmosphere* **2025**, *16*, 1297. https://doi.org/10.3390/atmos16111297

Copyright: © 2025 by the authors. Licensee MDPI, Basel, Switzerland. This article is an open access article distributed under the terms and conditions of the Creative Commons Attribution (CC BY) license (https://creativecommons.org/licenses/by/4.0/).

1. Introduction

Rossby waves [1] are a type of large-scale nonlinear wave generated by the Earth's rotational effects, with propagation driven by the latitudinal changes in the Coriolis force. These waves are crucial in atmospheric and oceanic dynamics, particularly in the study of large-scale circulation and climate variability [2,3]. A unique characteristic of Rossby solitary waves is their stability, which is strongly affected by topography and background flow conditions. As early as 1964, Long [4] derived that under the β-plane approximation, the amplitude evolution of Rossby waves satisfies the Korteweg–de Vries (KdV) equation. In 1966, Benney [5] extended Long's conclusion and additionally found that the speed of Rossby solitary waves is related to wave amplitude. Furthermore, Larsen [6] and Clarker [7] also studied the evolution of Rossby solitary wave amplitude, arriving at results similar to those of Long. The propagation of Rossby waves is influenced by topography, latitude variations, and atmospheric or oceanic density distribution, with their dynamics being particularly prominent in mid-to-high-latitude regions. As the primary form of meso- and planetary-scale disturbances in the atmosphere and oceans, Rossby waves play a key regulatory role in the variability of climate phenomena such as the tropospheric polar vortex and monsoon systems. It should be clarified that the tropospheric polar vortex initially forms due to polar cold sources and the Coriolis force, while Rossby waves do not directly drive its formation—instead, they modify the vortex's circulation intensity or induce its eccentricity through energy transport, consistent with the findings of Woollings [8].

Moreover, the slow propagation and long-periodic nature of Rossby waves allow them to affect atmospheric variability over extensive time and spatial scales [2,9].

Nonlinear dynamics have become a focal point in the study of Rossby waves. Research by Zhang [10] used the derivative expansion approach to investigate the dynamics of Rossby wave packets with topographic features, showing that topography has a profound impact on wave packet evolution. Yang et al. [11,12] introduced various nonlinear equations, including the Zakharov–Kuznetsov–Boussinesq–Ono (ZKBO) equation, to characterize Rossby solitary waves in three dimensions. The effects of topography, heating, and basic flow on these waves have been extensively investigated, significantly influencing wave propagation characteristics [13–16]. For instance, Yang et al. [17–20] explored how local topography can lead to baroclinic instability, while Vanneste [21] examined the finite damping of Rossby waves due to topographic influences. Han et al. [22] further studied the dynamics of Rossby algebraic solitary waves induced by large-scale topography, confirming that large-scale topographic features significantly modify the amplitude and propagation modes of these waves.

Zhang et al. [23] also employed the Ostrovsky hierarchy method to model the dynamics of nonlinear Rossby solitary waves, discovering that these waves exhibit similar stability characteristics. Additionally, Hou et al. [24] investigated the quartic *KdV* hierarchy of nonlinear Rossby waves and its dynamics, revealing the influence of topography on the nonlinear propagation of these waves. Wang et al. [25,26] studied solitary waves of nonlinear barotropic–baroclinic coherent structures and analyzed the impact of nonlinear interactions in the atmosphere and oceans.

The propagation of Rossby waves is inherently linked to environmental factors such as temperature gradients and atmospheric density distribution, which alter their dynamics [27,28]. Studies in recent decades, along with recent advances, have revealed the significance of algebraic solitary waves, which maintain stability and exhibit slow amplitude decay during propagation, making them particularly relevant in complex atmospheric and oceanic systems [29]. Zhang et al. [30] investigate the coherent structures resulting from nonlinear barotropic–baroclinic interactions in an unequal depth two-layer model. With the increasing effects of global warming and human activities, understanding the evolution of Rossby solitary waves has become critical for climate and weather predictions [31]. Recent advancements in numerical methods, such as the shooting method and Fourier spectral method, have facilitated the analysis of these waves under varying conditions [32]. Furthermore, studies have shown that the interaction between Rossby waves and other atmospheric phenomena, such as polar vortex dynamics, can have significant implications for weather variability.

Notably, Rossby algebraic solitary waves represent a special type of nonlinear solitary wave, characterized by slow amplitude decay and stable propagation. For algebraic solitary waves, the amplitude generally decays gradually with propagation distance, allowing for stable waveform maintenance over long distances and timescales. This stability enables Rossby algebraic solitary waves to persist even in complex environments, where they demonstrate certain propagation advantages in atmospheric and oceanic systems [33,34]. Studies have shown that these solitary waves can exhibit significant nonlinear responses when interacting with topography and temperature gradients and can adjust their propagation direction and amplitude in response to external disturbances [35–37]. These properties indicate that Rossby algebraic solitary waves not only hold substantial theoretical value in atmospheric and oceanic dynamics but may also play a critical role in practical climate forecasting [8,38].

To investigate the evolutionary characteristics of Rossby algebraic solitary waves, this paper starts from the shallow-water equations [39–41]. The shallow-water equations are a

set of fundamental equations that describe fluid movement under shallow-water conditions, applicable to atmospheric and oceanic fluid dynamics. Within the perturbation framework, the shallow-water equations can be simplified to reflect the nonlinear and dispersive characteristics of waves. Through perturbation expansion, we can derive the amplitude evolution equation from the shallow-water equations, leading to the BDO equation [42,43]. A recent study by Flamarion and Pelinovsky [44] has refined the nonlinear term coefficient in the BDO equation for weakly stratified fluids, establishing a quantitative relationship between topographic amplitude, spatial wavenumber, and the dispersion parameters of the equation. This work provides a direct theoretical foundation for incorporating the topographic function $\Omega(y)$ into the coefficient calibration of the BDO model in our study. The third part utilizes the PINNs method [45] to solve this equation and conduct an analysis. PINN is a novel approach that directly incorporates physical laws into the neural network training process, enabling the efficient solution of complex partial differential equations. For two-component BDO systems, Zhao and Qu [46] developed a perturbative symmetry-based discrete framework to mitigate numerical dispersion in Hilbert transform computations, though its computational efficiency diminishes when applied to scenarios with variable topographic parameters. Unlike traditional numerical methods, PINN does not rely on grid discretization but optimize the neural network parameters such that the network output satisfies the initial and boundary conditions, as well as naturally adheres to the physical constraints of the partial differential equations. This method has been proven effective in solving complex wave dynamics problems, such as the KdV equation and the NLS equation. By leveraging the physical constraints in the BDO equation, this method provides accurate solutions and deeper insights into Rossby wave dynamics. Finally, the study examines the effect of topography on the evolution of Rossby wave amplitudes.

2. Model and Hypotheses

The shallow-water equations [39] for a uniformly rotating fluid over variable bottom topography can be represented in the following form:

$$\begin{cases} \dfrac{\partial u_*}{\partial t_*} + u_* \dfrac{\partial u_*}{\partial x_*} + v_* \dfrac{\partial u_*}{\partial y_*} - (f_0 + \beta y_*) v_* = -g \dfrac{\partial \eta_*}{\partial x_*} \\ \dfrac{\partial v_*}{\partial t_*} + u_* \dfrac{\partial v_*}{\partial x_*} + v_* \dfrac{\partial v_*}{\partial y_*} + (f_0 + \beta y_*) u_* = -g \dfrac{\partial \eta_*}{\partial y_*} \\ \dfrac{\partial \eta_*}{\partial t_*} + \dfrac{\partial}{\partial x_*}[u_*(H_* + \eta_*)] + \dfrac{\partial}{\partial y_*}[v_*(H_* + \eta_*)] = 0, \end{cases} \tag{1}$$

where u_* , v_* , η_* , H_* , t_* , x_* and y_* stand for the eastward velocities, northward velocities, surface elevation, undisturbed water depth, time, eastward coordinate, and northward coordinate, respectively. In this work, all physical quantities with a superscript "$*$" denote dimensional quantities. Also, mark the lower part with asterisks as dimensional variables. $f = f_0 + \beta y_*$, g are defined as the Coriolis parameter and gravitational acceleration, respectively. The β parameter represents the latitudinal gradient of the Coriolis parameter, and

$$\zeta_* = \frac{\partial v_*}{\partial x_*} - \frac{\partial u_*}{\partial y_*} \tag{2}$$

is defined as relative vorticity. The expression

$$\frac{\mathrm{D}}{\mathrm{D}t_*}\left[\frac{\zeta_* + f}{H_* + \eta_*}\right] = 0 \tag{3}$$

is for conservation of potential vorticity, where $\mathrm{D}/\mathrm{D}t_* = \frac{\partial}{\partial t_*} + u_*\frac{\partial}{\partial x_*} + v_*\frac{\partial}{\partial y_*}$ stands for the derivative of matter along the path of the particle. Because of the continuity equation, we can set up the following stream function Ψ_*,

$$\frac{\partial \Psi_*}{\partial x_*} = H_* v_*, \quad \frac{\partial \Psi_*}{\partial y_*} = -H_* u_*. \tag{4}$$

By substituting Equation (4) into Equation (2) we get the relative vorticity

$$\zeta_* = \frac{1}{H_*}\nabla_*^2 \Psi_* - \frac{1}{H_*^2}\nabla_* \Psi_* \cdot \nabla_* H_*, \tag{5}$$

where ∇_* is the gradient operator and $\nabla_*^2 = \frac{\partial^2}{\partial x_*^2} + \frac{\partial^2}{\partial y_*^2}$ stands for the Laplace operator. The first and second terms of Equation (5) are the vertical water column vorticity and topographic vorticity, respectively. This is the result of the advection function interacting with the gradient of the bottom topography. This factor is highly relevant when both the slope of the bed and the volume of material transported are large and nearly the same, which is often seen on continental slopes.

Substitute Equation (5) into Equation (3) to get

$$\begin{aligned} &\frac{\partial}{\partial t_*}\nabla_*^2 \Psi_* - \frac{1}{H_*}\frac{\partial}{\partial t_*}\nabla_* \Psi_* \cdot \nabla_* H_* + H_* J_*(\Psi_*, \frac{f_0}{H_*}) + \frac{1}{H_*} J_*(\Psi_*, \nabla_*^2 \Psi_*) + \beta \frac{\partial \Psi_*}{\partial x_*} \\ &- \frac{1}{H_*^2} J_*(\Psi_*, \nabla_* \Psi_* \cdot \nabla_* H_*) + 3\frac{\nabla_* \Psi_* \cdot \nabla_* H_*}{H_*^3} J_*(\Psi_*, H_*) - 2\frac{\nabla_*^2 \Psi_*}{H_*^2} J_*(\Psi_*, H_*) = 0, \end{aligned} \tag{6}$$

where $J_*(a_*, b_*) = \frac{\partial a_*}{\partial x_*}\frac{\partial b_*}{\partial y_*} - \frac{\partial a_*}{\partial y_*}\frac{\partial b_*}{\partial x_*}$ is the Jacobian operator. The first term in Equation (6) represents the dynamic vorticity rate of change for the barotropic stream function, indicating the effect of the vertically integrated rotation of the water column. The second term represents the temporal rate of change in topographic vorticity. In the third term, we observe the deviation of the flow relative to the line of f_0/H_*. The fourth term denotes the nonlinear interaction or advection of the dynamic vorticity. The fifth term represents the variation in planetary vorticity. The sixth term captures the advection effect in topographic vorticity. The seventh term describes the advection of topographic vorticity across an inclined bottom. The eighth term denotes the advection of dynamic vorticity along an inclined bottom.

We designate Equation (6) as the topographic potential vorticity equation. Following this, we perform the nondimensionalization of Equation (6) using the characteristic scales of horizontal length L, characteristic time scale T, characteristic horizontal velocity scale U, and characteristic vertical depth scale H_0. Setting the depth as $H = H_*/H_0 = 1 - \delta\eta_B$, we let η_B represent the nondimensional bottom topography. Additionally, the small nondimensional number is assigned to $\omega = \frac{1}{f_0 T}$, $\delta = \frac{|(\frac{\partial H}{\partial y})L|}{H_0}$, $\widehat{\beta} = \frac{\beta L}{f_0}$, $R_0 = \frac{U}{f_0 L}$ and the mass transport function takes the nondimensional form of $H_0 UL$. As a result, we arrive at the following nondimensional form

$$\begin{aligned} &\omega\frac{\partial}{\partial t}\nabla^2 \Psi + \frac{\delta\omega}{1-\delta\eta_B}\frac{\partial}{\partial t}\nabla \Psi \cdot \nabla \eta_B + \frac{\delta}{1-\delta\eta_B} J(\Psi, \eta_B) + \frac{R_0}{1-\delta\eta_B} J(\Psi, \nabla^2 \Psi) \\ &+ \widehat{\beta}\frac{\partial \Psi}{\partial x} + \frac{\delta R_0}{(1-\delta\theta_B)^2} J(\Psi, \nabla \Psi \cdot \nabla \eta_B) + 3\frac{\delta^2 R_0}{(1-\delta\eta_B)^3}\nabla \Psi \cdot \nabla \eta_B J(\Psi, \eta_B) \\ &+ 2\frac{\delta R_0}{(1-\delta\eta_B)^2}\nabla^2 \Psi J(\Psi, \eta_B) = 0. \end{aligned} \tag{7}$$

Because the geomorphological concept underpins the scaling factor $\omega \sim \delta \sim R_0$, ($\widehat{\beta} \ll 1$), we obtain the nondimensional form of the governing equations with the topography

$$\begin{aligned} &\frac{\partial}{\partial t}\nabla^2\Psi + \delta\frac{\partial}{\partial t}\nabla\Psi\cdot\nabla\eta_B + (1+\delta\eta_B+2\delta\nabla^2\Psi)J(\Psi,\eta_B) \\ &+ (1+\delta\eta_B)J(\Psi,\nabla^2\Psi) + \delta J(\Psi,\nabla\Psi\cdot\nabla\eta_B) + \beta\frac{\partial\Psi}{\partial x} = 0. \end{aligned} \tag{8}$$

The basic stream function is taken as the zonal flow

$$\Psi(y) = -\int_0^y [\overline{U}(s) - c_0]\mathrm{d}s, \tag{9}$$

where c_0 denotes the wave speed. Next, the topography will be established as

$$\eta_B(y) = \varepsilon\Omega(y), \tag{10}$$

where ε is the small parameter used to measure the extent of nonlinearity. Thus, the total stream function is given by

$$\psi(x,y,t) = \Psi(y) + \varepsilon\psi'(x,y,t) = -\int_0^y [\overline{U}(s) - c_0]\mathrm{d}s + \varepsilon\psi'(x,y,t), \tag{11}$$

By neglecting the prime on the perturbation stream function ψ' without loss of confusion, and substituting Equations (10) and (11) into (8), we obtain the following equation:

$$\begin{aligned} &\left[\frac{\partial}{\partial t} + (\overline{U}-c_0)\frac{\partial}{\partial x} + \varepsilon\delta\Omega(\overline{U}-c_0)\frac{\partial}{\partial x}\right]\nabla^2\psi + \varepsilon\delta\frac{\partial}{\partial t}(\frac{\partial\psi}{\partial y}\Omega') \\ &+ \varepsilon(1+\varepsilon\delta\Omega+2\varepsilon\delta\nabla^2\psi-2\delta\overline{U}')\frac{\partial\psi}{\partial x}\Omega' + \varepsilon(1+\varepsilon\delta\Omega)J(\psi,\nabla^2\psi) \\ &+ (\beta - \frac{d^2\overline{U}}{dy^2})\frac{\partial\psi}{\partial x} - \varepsilon\delta\Omega\frac{d^2\overline{U}}{dy^2}\frac{\partial\psi}{\partial x} - \varepsilon\delta\frac{\partial\psi}{\partial x}\frac{\partial}{\partial y}[(\overline{U}-c_0)\Omega'] \\ &+ \varepsilon\left[\varepsilon\delta\frac{\partial\psi}{\partial x}\frac{\partial}{\partial y} + \delta(\overline{U}-c_0)\frac{\partial}{\partial x} - \varepsilon\delta\frac{\partial\psi}{\partial y}\frac{\partial}{\partial x}\right]\frac{\partial\psi}{\partial y}\Omega' = 0, \end{aligned} \tag{12}$$

where $\Omega' = \frac{\mathrm{d}\Omega(y)}{\mathrm{d}y}$, and Ω represents the dimensionless bottom topography profile function, while the symbol Ω' with a dot denotes the first-order partial derivative of Ω with respect to its argument y. Equation (12) describes the dynamics in the region $[-L, L]$, based on *Ono*'s boundary conditions, which allow us to neglect the topography in the external region and derive the relevant equations for the case where the Coriolis force $f = 0$:

$$\left[\frac{\partial}{\partial t} + (\overline{U}_1 - c_0)\frac{\partial}{\partial x}\right]\nabla^2\psi + \varepsilon J(\psi,\nabla^2\psi) = 0,\ y > L \tag{13}$$

$$\left[\frac{\partial}{\partial t} + (\overline{U}_2 - c_0)\frac{\partial}{\partial x}\right]\nabla^2\psi + \varepsilon J(\psi,\nabla^2\psi) = 0,\ y < -L. \tag{14}$$

In Equation (12), the variables x, y, and t undergo the Gardner–Morikawa transformation

$$X = \varepsilon x,\ T = \varepsilon^2 t,\ y = y. \tag{15}$$

By substituting Equation (15) into Equation (12), we get

$$\begin{aligned}
&\left[\varepsilon\frac{\partial}{\partial T}+(\overline{U}-c_0)\frac{\partial}{\partial X}+\varepsilon\delta\Omega(\overline{U}-c_0)\frac{\partial}{\partial X}\right](\varepsilon^2\frac{\partial^2\psi}{\partial X^2}+\frac{\partial^2\psi}{\partial y^2})+\varepsilon^2\delta\frac{\partial}{\partial T}\frac{\partial\psi}{\partial y}\Omega'\\
&+\varepsilon\left[1+\varepsilon\delta\Omega+2\varepsilon\delta(\varepsilon^2\frac{\partial^2\psi}{\partial X^2}+\frac{\partial^2\psi}{\partial y^2})-2\delta\overline{U}'\right]\frac{\partial\psi}{\partial X}\Omega'+\varepsilon^3(\frac{\partial\psi}{\partial X}\frac{\partial}{\partial y}-\frac{\partial\psi}{\partial y}\frac{\partial}{\partial X})\frac{\partial^2\psi}{\partial X^2}\\
&+\varepsilon(\frac{\partial\psi}{\partial X}\frac{\partial}{\partial y}-\frac{\partial\psi}{\partial y}\frac{\partial}{\partial X})\frac{\partial^2\psi}{\partial y^2}+\varepsilon^4\delta\Omega(\frac{\partial\psi}{\partial X}\frac{\partial}{\partial y}-\frac{\partial\psi}{\partial y}\frac{\partial}{\partial X})\frac{\partial^2\psi}{\partial X^2}\\
&+\varepsilon^2\delta\Omega(\frac{\partial\psi}{\partial X}\frac{\partial}{\partial y}-\frac{\partial\psi}{\partial y}\frac{\partial}{\partial X})\frac{\partial^2\psi}{\partial y^2}+\overline{\beta}(y)\frac{\partial\psi}{\partial X}-\varepsilon\delta\Omega\frac{\mathrm{d}^2\overline{U}}{\mathrm{d}y^2}\frac{\partial\psi}{\partial X}\\
&-\varepsilon\delta\frac{\partial\psi}{\partial X}\frac{\partial}{\partial y}[(\overline{U}-c_0)\Omega']+\varepsilon\left[\varepsilon\delta\frac{\partial\psi}{\partial X}\frac{\partial}{\partial y}+\delta(\overline{U}-c_0)\frac{\partial}{\partial X}-\varepsilon\delta\frac{\partial\psi}{\partial y}\frac{\partial}{\partial X}\right]\frac{\partial\psi}{\partial y}\Omega'=0.
\end{aligned}\tag{16}$$

In Equation (16), $\overline{\beta}(y)=\beta-\dfrac{\mathrm{d}^2\overline{U}}{\mathrm{d}y^2}$. Expand $\psi(X,y,T)$ in terms of the small parameter ε

$$\psi(X,y,T)=\psi_0(X,y,T)+\varepsilon\psi_1(X,y,T)+O(\varepsilon^2).\tag{17}$$

Equation (17) is substituted into Equation (16) to obtain the equations of the reduced perturbation problems of each other. The equation in the zeroth order of the small value of ε is

$O(\varepsilon^0)$:

$$\frac{\partial}{\partial X}(\frac{\partial^2\psi_0}{\partial y^2})+\frac{\overline{\beta}(y)}{\overline{U}-c_0}\frac{\partial\psi_0}{\partial X}=0,\tag{18}$$

where $\overline{U}-c_0\neq0$. Assuming that $\rho\psi_0\to0$, as $y\to\infty$, then the following form holds:

$$\psi_0=A(X,T)\phi(y).\tag{19}$$

Substitute (19) into Equation (18) to get

$$(\frac{\mathrm{d}^2}{\mathrm{d}y^2}+\frac{\overline{\beta}(y)}{\overline{U}-c_0})\phi(y)=0.\tag{20}$$

In order to understand how wave amplitude evolves with time, we continue to solve and derive the first-order equation, which is

$O(\varepsilon^1)$:

$$\begin{aligned}
&\frac{\partial}{\partial X}(\frac{\partial^2\psi_1}{\partial y^2})+\frac{\overline{\beta}(y)}{\overline{U}-c_0}\frac{\partial\psi_1}{\partial X}=(\frac{\partial A}{\partial T}-A\frac{\partial\phi}{\partial y}\frac{\partial A}{\partial X})\frac{\overline{\beta}(y)}{(\overline{U}-c_0)^2}\phi(y)\\
&+A\frac{\partial A}{\partial X}\frac{\phi^2(y)}{\overline{U}-c_0}\frac{\mathrm{d}}{\mathrm{d}y}(\frac{\overline{\beta}(y)}{\overline{U}-c_0})+\delta\Omega\frac{\partial A}{\partial X}\frac{\overline{\beta}(y)}{\overline{U}-c_0}\phi(y)+(2\delta\overline{U}'-1)\frac{\phi(y)}{\overline{U}-c_0}\frac{\partial A}{\partial X}\Omega'\\
&+\delta\frac{\phi(y)}{\overline{U}-c_0}\frac{\partial A}{\partial X}\overline{U}'\Omega'+\delta\phi(y)\frac{\partial A}{\partial X}\Omega''-\delta\frac{\partial A}{\partial X}\frac{\partial\phi}{\partial y}\Omega'+\delta\Omega\frac{\phi(y)}{\overline{U}-c_0}\frac{\mathrm{d}^2\overline{U}}{\mathrm{d}y^2}\frac{\partial A}{\partial X}.
\end{aligned}\tag{21}$$

The non-singular solution condition is required to be

$$\begin{aligned}
&\frac{\partial}{\partial X}\left[\phi(y)\frac{\partial \psi_1}{\partial y}-\psi_1\frac{\partial \phi(y)}{\partial y}\right]|_{-L}^{L}=\frac{\partial A}{\partial T}\int_{-L}^{L}\frac{\overline{\beta}(y)}{(\overline{U}-c_0)^2}\phi^2(y)\mathrm{d}y\\
&-A\frac{\partial A}{\partial X}\int_{-L}^{L}\frac{\partial \phi}{\partial y}\frac{\overline{\beta}(y)}{(\overline{U}-c_0)^2}\phi^2(y)\mathrm{d}y+A\frac{\partial A}{\partial X}\int_{-L}^{L}\frac{\phi^3(y)}{\overline{U}-c_0}\frac{\mathrm{d}}{\mathrm{d}y}(\frac{\overline{\beta}(y)}{\overline{U}-c_0})\mathrm{d}y\\
&+\delta\frac{\partial A}{\partial X}\int_{-L}^{L}\Omega\frac{\overline{\beta}(y)}{\overline{U}-c_0}\phi^2(y)\mathrm{d}y+3\delta\frac{\partial A}{\partial X}\int_{-L}^{L}\frac{\phi^2(y)}{\overline{U}-c_0}\overline{U}'\Omega'\mathrm{d}y\\
&-\frac{\partial A}{\partial X}\int_{-L}^{L}\frac{\phi^2(y)}{\overline{U}-c_0}\Omega'\mathrm{d}y+\delta\frac{\partial A}{\partial X}\int_{-L}^{L}\phi^2(y)\Omega''\mathrm{d}y-\delta\frac{\partial A}{\partial X}\int_{-L}^{L}\phi(y)\frac{\partial \phi}{\partial y}\Omega'\mathrm{d}y\\
&+\delta\frac{\partial A}{\partial X}\int_{-L}^{L}\Omega\frac{\phi^2(y)}{\overline{U}-c_0}\frac{\mathrm{d}^2\overline{U}}{\mathrm{d}y^2}\mathrm{d}y.
\end{aligned}\tag{22}$$

The left hand of Equation (20) is determined by the external (13), (14). Since the external disturbance is generated through the inside, we have

$$\xi=x,\ T=\varepsilon^2 t\tag{23}$$

$$\psi(x,y,t)=\varepsilon\widetilde{\psi}(\xi,y,T).\tag{24}$$

Substituting (23), (24) into (13), (14) gives the lowest-order external equation

$$(\overline{U}_1-c_0)\frac{\partial}{\partial \xi}(\frac{\partial^2\widetilde{\psi}}{\partial \xi^2}+\frac{\partial^2\widetilde{\psi}}{\partial y^2})=0,\ y>L\tag{25}$$

$$(\overline{U}_2-c_0)\frac{\partial}{\partial \xi}(\frac{\partial^2\widetilde{\psi}}{\partial \xi^2}+\frac{\partial^2\widetilde{\psi}}{\partial y^2})=0,\ y<-L,\tag{26}$$

where $\overline{U}_1-c_0\neq 0,\ \overline{U}_2-c_0\neq 0$. According to Ono [47,48], it is easy to obtain (25), (26)

$$\begin{cases}\dfrac{\partial^2\widetilde{\psi}}{\partial \xi^2}+\dfrac{\partial^2\widetilde{\psi}}{\partial y^2}=0\\ \widetilde{\psi}\to 0,\ |y|\to\infty.\end{cases}\tag{27}$$

The soulution of (27) is

$$\begin{cases}\widetilde{\psi}(\xi,y,T)=\dfrac{1}{\pi}\mathscr{P}\displaystyle\int_{-\infty}^{+\infty}\widetilde{\psi}(\xi',L,T)\frac{(y-L)}{(\xi-\xi')^2+(y-L)^2}\mathrm{d}\xi',\ y>L\\ \widetilde{\psi}(\xi,y,T)=\dfrac{-1}{\pi}\mathscr{P}\displaystyle\int_{-\infty}^{+\infty}\widetilde{\psi}(\xi',-L,T)\frac{y+L}{(\xi-\xi')^2+(y+L)^2}\mathrm{d}\xi',\ y<-L,\end{cases}\tag{28}$$

where $\mathscr{P}$ represents the above integral principal value. Upon differentiating with respect to y, we find

$$\begin{cases}\dfrac{\partial\widetilde{\psi}(\xi,y,T)}{\partial y}=\dfrac{1}{\pi}\mathscr{P}\displaystyle\int_{-\infty}^{+\infty}\widetilde{\psi}(\xi',L,T)\frac{(\xi-\xi')^2-(y-L)^2}{[(\xi-\xi')^2+(y-L)^2]^2}\mathrm{d}\xi',\ y>L\\ \dfrac{\partial\widetilde{\psi}(\xi,y,T)}{\partial y}=\dfrac{-1}{\pi}\mathscr{P}\displaystyle\int_{-\infty}^{+\infty}\widetilde{\psi}(\xi',-L,T)\frac{(\xi-\xi')^2-(y+L)^2}{[(\xi-\xi')^2+(y+L)^2]^2}\mathrm{d}\xi',\ y<-L.\end{cases}\tag{29}$$

The inner solution in the y direction is smooth at L, $-L$, and therefore at $O(\varepsilon^1)$, it has

$$\begin{cases}\psi_0(X,L,T)+\varepsilon\psi_1(X,L,T)=\widetilde{\psi}(\xi,L,T)+O(\varepsilon)\\ \psi_0(X,-L,T)+\varepsilon\psi_1(X,-L,T)=\widetilde{\psi}(\xi,-L,T)+O(\varepsilon)\end{cases}\tag{30}$$

and

$$\begin{cases} \dfrac{\partial \psi_0(X,L,T)}{\partial y} + \varepsilon \dfrac{\partial \psi_1(X,L,T)}{\partial y} = \dfrac{\partial \widetilde{\psi}(\xi,L,T)}{\partial y} + O(\varepsilon) \\ \dfrac{\partial \psi_0(X,-L,T)}{\partial y} + \varepsilon \dfrac{\partial \psi_1(X,-L,T)}{\partial y} = \dfrac{\partial \widetilde{\psi}(\xi,-L,T)}{\partial y} + O(\varepsilon). \end{cases} \tag{31}$$

As given by (19) and (30),

$$\begin{cases} A(X,T)\phi(L) = \widetilde{\psi}(\xi,L,T) \\ A(X,T)\phi(-L) = \widetilde{\psi}(\xi,-L,T) \\ \psi_1(X,L,T) = 0 \\ \psi_1(X,-L,T) = 0. \end{cases} \tag{32}$$

Plugging (30) into (29) leads to

$$\begin{cases} \dfrac{\partial \widetilde{\psi}(\xi,L,T)}{\partial y} = -\varepsilon\phi(L)\dfrac{\partial}{\partial X}\mathscr{H}(A(X,T)) \\ \dfrac{\partial \widetilde{\psi}(\xi,-L,T)}{\partial y} = \varepsilon\phi(-L)\dfrac{\partial}{\partial X}\mathscr{H}(A(X,T)), \end{cases} \tag{33}$$

where $\mathscr{H}(A(X,T)) = \dfrac{1}{\pi}\mathscr{P}\displaystyle\int_{-\infty}^{+\infty}\frac{A(X',T)}{X-X'}\mathrm{d}X'$ represents the Hilbert transform of $A(X,T)$. Using (31) and (33), we can obtain

$$\begin{cases} \dfrac{\mathrm{d}\phi}{\mathrm{d}y}|_{y=L} = 0 \\ \dfrac{\mathrm{d}\phi}{\mathrm{d}y}|_{y=-L} = 0 \end{cases} \tag{34}$$

and

$$\begin{cases} \dfrac{\partial \psi_1(X,L,T)}{\partial y} = -\phi(L)\dfrac{\partial}{\partial X}\mathscr{H}(A(X,T)) \\ \dfrac{\partial \psi_1(X,-L,T)}{\partial y} = \phi(-L)\dfrac{\partial}{\partial X}\mathscr{H}(A(X,T)). \end{cases} \tag{35}$$

Substituting (32), (34), and (35) into (22) leads to

$$\frac{\partial A}{\partial T} + (Q-D)A\frac{\partial A}{\partial X} + (F+M-V+G-E+Z)\frac{\partial A}{\partial X} + S\frac{\partial^2 \mathscr{H}(A)}{\partial X^2} = 0. \tag{36}$$

To accurately characterize the topographic modulation effect on Rossby waves, the flow field is partitioned into inner and outer regions based on the Ono boundary conditions, with their respective dynamical characteristics specified as follows:

- Inner Region: Spatially defined as the zone of significant topographic influence, $y \in [-L, L]$, where L represents the characteristic topographic scale (set here as $L = 5 \times 10^5$ m, consistent with the half-width of mid-latitude mountain systems). The core dynamical process in this region is the topography–vorticity interaction: the topographic vorticity term modulates the evolution of relative vorticity, thereby influencing the nonlinear growth and decay of Rossby wave amplitude.
- Outer Region: Defined as the zone where topographic effects are negligible, $y > L$ or $y < -L$. Here, the topographic height $\Omega(y) \to 0$, and the dominant dynamics reduce to dispersion-driven propagation in the absence of topography. The flow evolution

is governed solely by the Coriolis force and background flow, leading to a linear wave equation free of topographic terms. The solution in this region is expressed in terms of a principal value integral (Equation (28)). The outer solution must satisfy matching conditions at the boundaries $y = \pm L$ with the inner solution—specifically, the continuity of the stream function and its normal derivative—thereby providing rigorous boundary constraints for the amplitude evolution in the inner region.

Equation (36) is known as the *BDO* equation. As indicated by the parameters, the coefficients of the equation depend on $\overline{\beta}(y)$, $\overline{U}(y)$, and the terrain $\Omega(y)$. The parameters associated with terrain variations modify the linear terms, thus influencing the dispersive properties of Rossby solitary waves, and the parameters σ, D, S, Q, F, M, V, G, E, and Z are specified in Appendix A. In the limiting case of vanishing topographic influence ($\delta = 0$), Equation (36) reduces to the classical *Ono* equation [47] as all topographic coupling terms (specifically coefficients F, M, and G containing $\Omega(y)$) become negligible. Under the condition of suppressed dispersive effects ($S = 0$), the equation simplifies to a *KdV*-type [4] formulation with topographic modulation, aligning with the topographic Rossby wave structure previously established by Long. The derivation assumes shallow-water conditions ($H_* \ll L_*$); β-plane framework ($\beta y_* \ll f_0$); and weak nonlinearity ($u_* \ll \overline{U}_*$). The convergence of the perturbation expansion is ensured by $\widehat{\beta} \ll 1$, while all dimensional parameters are constrained by observational data from mid- and high-latitude atmospheric regimes.

3. Results and Discussion

Next, we set $\Omega(y)$ to be

$$\Omega(y) = B\sin(\omega y), \tag{37}$$

where B and ω are set as constants, B represents the topographic amplitude, and ω is the angular velocity of the wave, respectively. Then we have $\overline{U}(L) = \overline{U}_1$, $\overline{U}(-L) = \overline{U}_2$, and

$$\overline{U}(y) = (\overline{U}_1 - \overline{U}_2)\cos(\omega y) + \frac{\overline{U}_1 - \overline{U}_2}{2}. \tag{38}$$

And for that, we get

$$\overline{\beta}(y) = \beta - \frac{\mathrm{d}^2\overline{U}}{\mathrm{d}y^2} = \beta + (\overline{U}_1 - \overline{U}_2)\omega^2\cos(\omega y). \tag{39}$$

Substituting (38) and (39) into Equation (20) yields

$$\phi''(y) + \frac{\beta + (\overline{U}_1 - \overline{U}_2)\omega^2\cos(\omega y)}{(\overline{U}_1 - \overline{U}_2)\cos(\omega y) + \frac{\overline{U}_1 - \overline{U}_2}{2} - c_0}\phi(y) = 0. \tag{40}$$

A PINN is a numerical method. The core idea of a PINN is to incorporate the physical constraints of the PDE into the loss function, thereby training the neural network. The basic procedures for solving differential equations with the PINN method are as follows:

- First of all, a neural network $\widehat{u}(x, \theta)$ has to be constructed as a surrogate model for the solution of the differential equation.
- The training set of the neural network needs to be specified (typically including two sets for the spatiotemporal domain and boundary conditions).
- The loss function needs to be defined by means of the weighted sum of the L_2 norms of the residuals of the equation and the boundary conditions.
- Minimize the loss function L to train the neural network and acquire the optimal values of the parameters.

In the process of solving the equation, the time domain is defined as $t \in [0, 500]$ and the spatial domain is $x \in [-200, 200]$. We build a neural network that consists of three hidden layers, with 100 neurons in each layer. The tanh function is chosen as the activation function for the neural network, and the weights of all layers of the neural network are initialized via the Xavier initialization approach. When it comes to the training process, we randomly sample 3000 training-data coordinates inside the equation by using the Latin hypercube sampling technique. Meanwhile, 200 training-data coordinates are sampled from both the initial conditions and the boundary conditions. Subsequently, the Adam algorithm is utilized to perform 40,000 iterations on the neural network. Finally, the trained neural network is utilized to compute the predicted values of the equation's solution at the given coordinates. These predicted values are then compared with the analytical solutions of the equation. Next, Equation (40) will be solved using the PINN method.

Substitute the obtained $\phi(y)$ (as shown in Figure 1) and Equations (37)–(39) into the respective parameters in Appendix A to obtain the parameters σ, D, S, Q, F, M, V, G, E, and Z, where $\delta = 0.01$.

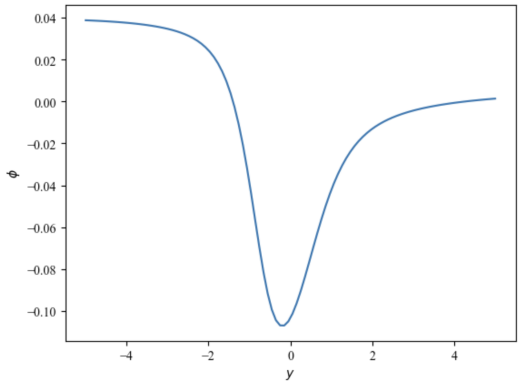

Figure 1. Numerical solution of Equation (40), where $\overline{U}_1 = 5 \times \sin(1)$, $\overline{U}_2 = 2 \times \sin(1)$, $c_0 = 1$, $\omega = 4$, $\beta = 1.98 \times 10^{-10}$.

Substitute the given parameters and let $\varepsilon = 0.5$ into the soulution of the amplitude A in Equation (36), where A_0 is the initial amplitude and is set to 2.5.

The solution to Equation (36) is also obtained using the PINN method. Figure 2 provides an overview of the PINN algorithm results, where Figure 2a displays the loss function L, Figure 2b shows the heatmap of absolute error, Figure 2c illustrates the equation's exact solution, and Figure 2d shows the solution obtained by the PINN. In the solution process of this paper, the parameter values used are $\varepsilon = 0.5$, $\delta = 0.01$, $B = 3$, and $\omega = 4$. A relative L_2 error of 3.58×10^{-2} was achieved, which indicates that the PINN can closely capture the soliton chasing behavior of the equation. Here, $loss$: total loss function of the PINN; $loss_u$: loss term corresponding to initial and boundary conditions; $loss_r$: loss term representing the residual of the BDO equation.

Figure 3 shows the solution of the BDO equation. This equation is often used to describe long waves in shallow water, such as Rossby waves in the atmosphere. From the graph, we can observe that the amplitude $A(x, t)$ reaches peak values at certain points of x and t, while it gradually decreases in other regions. This suggests that the amplitude of Rossby waves fluctuates as influenced by terrain variations. Higher amplitude regions might correspond to areas where terrain elevations or wave enhancements occur, while lower amplitude areas may indicate regions where the impact of terrain on wave dynamics is weaker. The variation of amplitude with t also shows the propagation and evolution of waves, likely linked to the influence of terrain on fluid dynamics. It should be noted that the current study focuses on presenting the qualitative laws of amplitude evolution

of topographic Rossby algebraic solitary waves, and has not yet fully completed the quantitative calculation of wave velocity under different parameters. Additionally, the quantitative characterization of the parameter influence on wave amplitude still needs improvement, resulting in the unclear presentation of the regulatory effect of parameters on wave velocity and the specific influence degree on wave amplitude. Future studies will further optimize the wave velocity extraction method, supplement the quantitative analysis of amplitude differences under multiple parameter sets, and systematically clarify the regulatory mechanism of parameters on wave amplitude and wave velocity to improve the conclusions of this study.

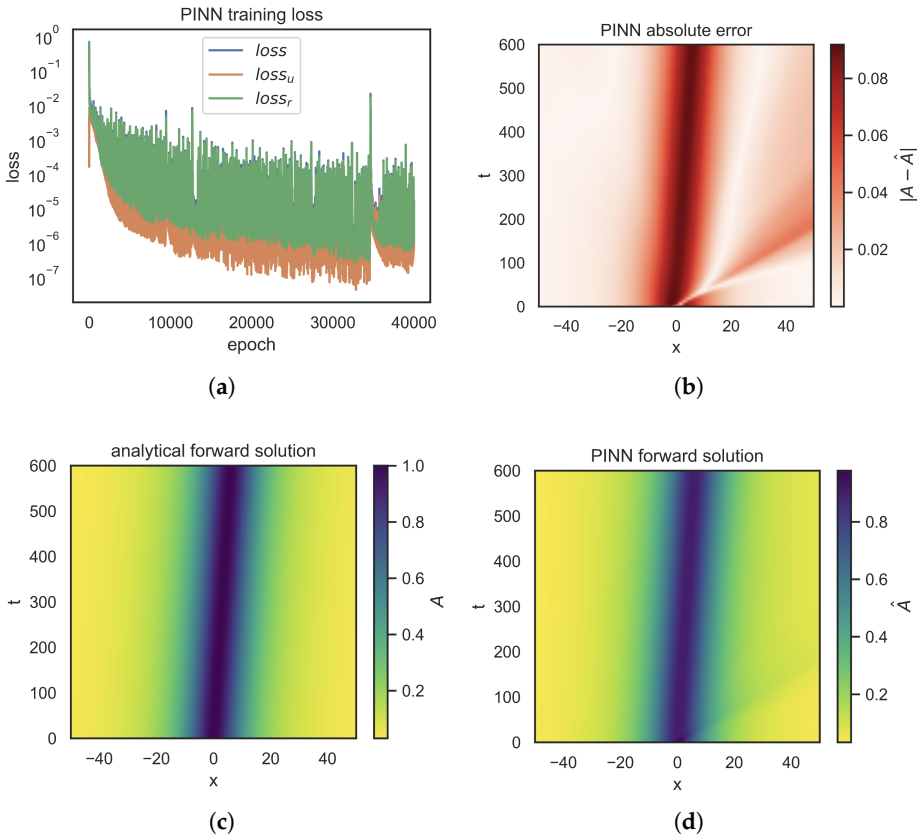

Figure 2. The PINN method applied to the amplitude A, (**a**) the variation process of the loss function; (**b**) the absolute error; (**c**) the exact solution of the equation; (**d**) the solution obtained by the PINN.

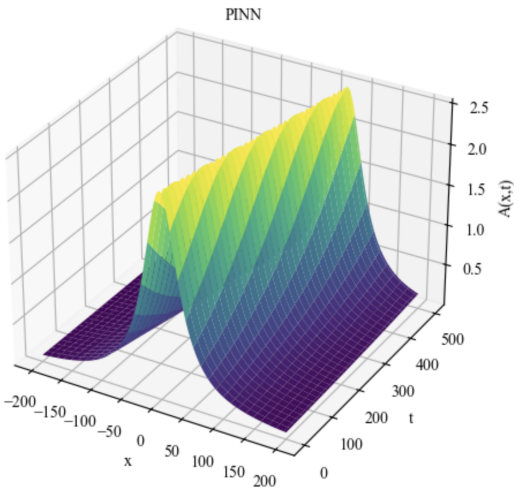

Figure 3. Solution for amplitude A.

Figures 4 and 5 illustrate how terrain parameters affect the Rossby wave's amplitude A over time, with epsilon fixed at 0.5 and B values of 3, 4, and 5, and ω values of 4, 5, and 6. The figures indicate that changes in B and ω influence wave speed, thus impacting terrain and, in turn, amplitude A. Higher B and ω values correspond to a greater effect on wave speed. Over time, the rightward movement becomes faster, concentrating energy and enhancing wave propagation speed.

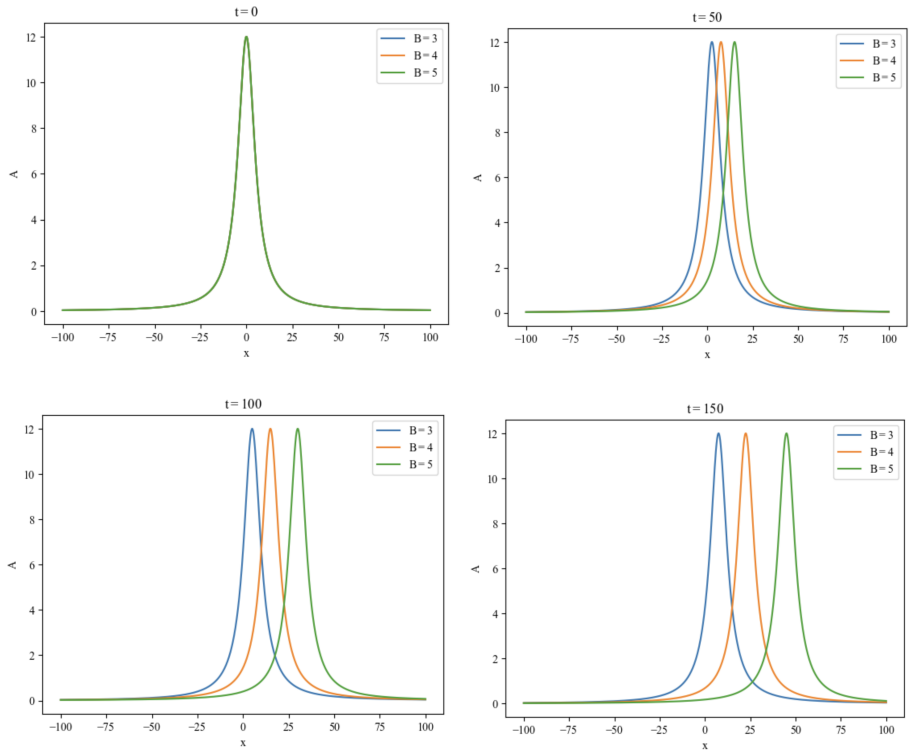

Figure 4. Chart of Rossby wave amplitude A relative to wave amplitude B over different time periods.

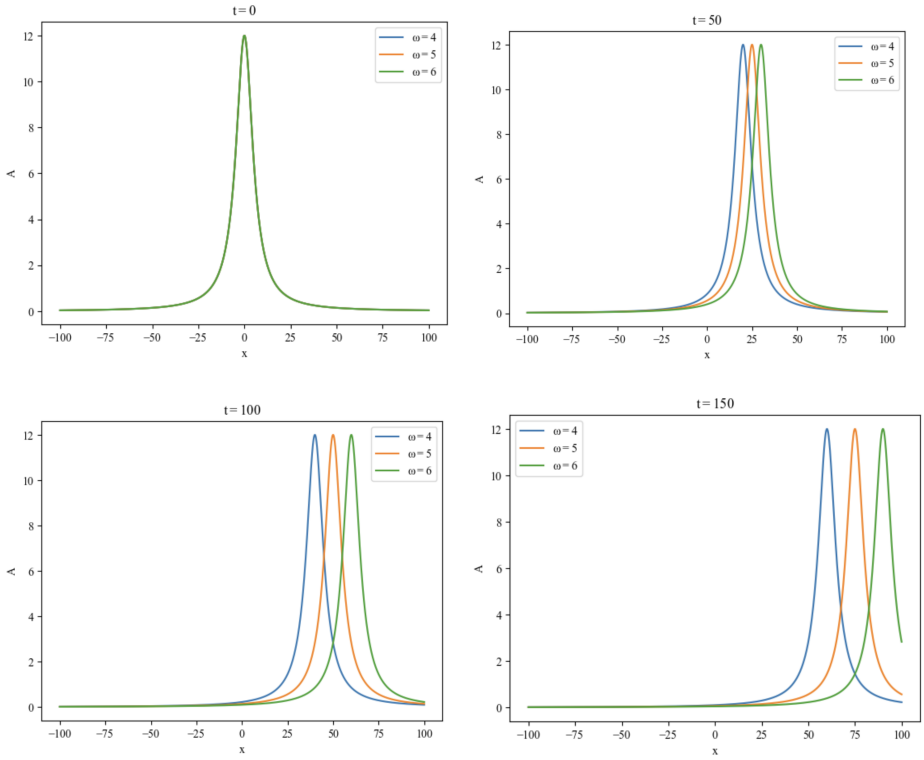

Figure 5. Diagram of the changes in amplitude A and angular velocity of the Rossby wave over time.

Figure 6 displays contour maps of the perturbation stream function ψ_0 at different time instants under $\delta = 0.01$. The spatiotemporal evolution of the contour structures reflects variations in the topographic configuration of the Rossby solitary wave. At $t = 0$, the stream function contours exhibit symmetric distribution centered along the x-axis, with well-defined peaks and troughs indicating maximum wave amplitude and concentrated topographic influence, characteristic of a canonical Rossby wave pattern.

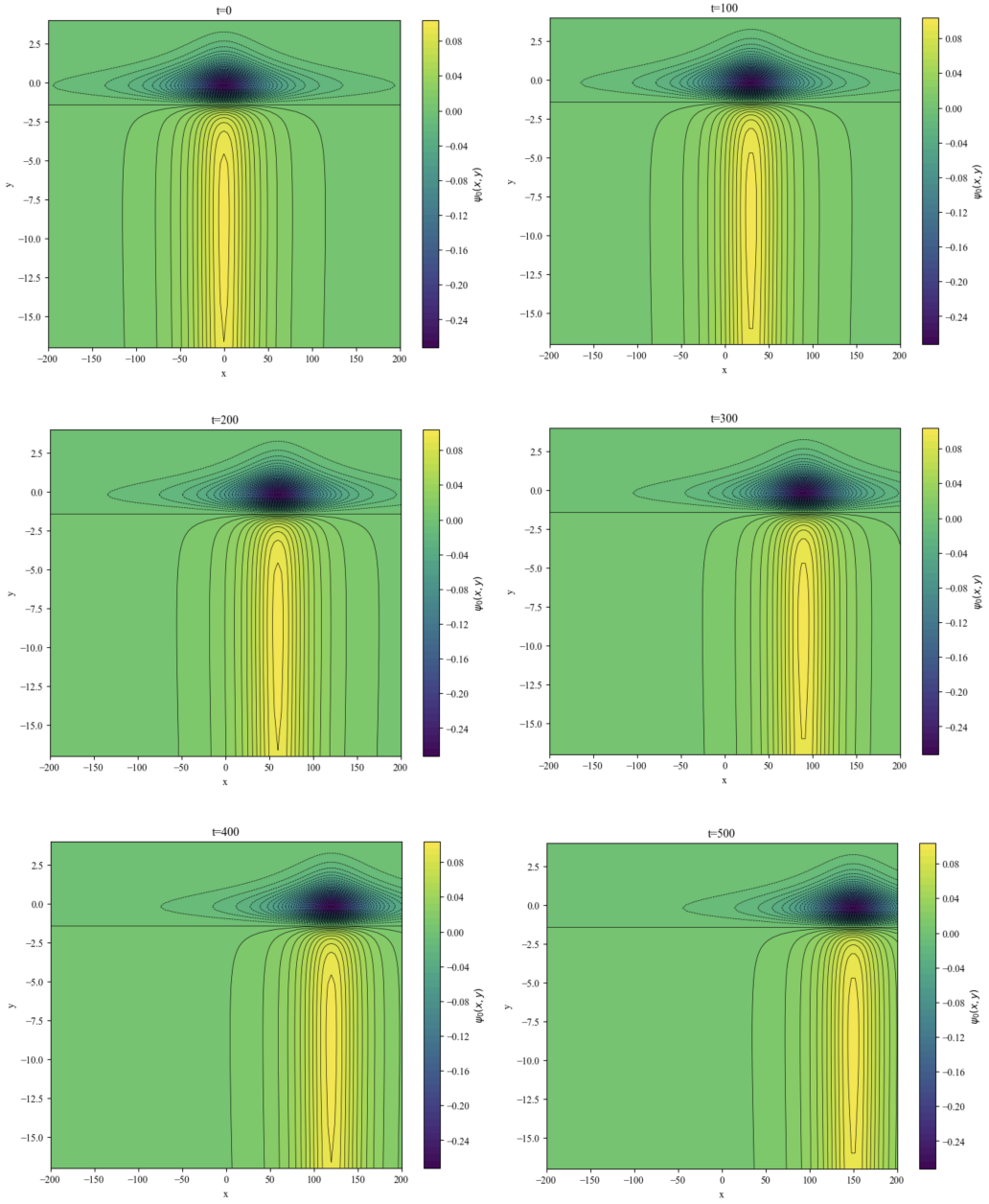

Figure 6. Propagation of the perturbation stream function.

As time advances, the wave structure shifts rightward while retaining its morphological stability—suggesting efficient energy propagation without significant structural distortion. This stable translation likely arises from the dynamic balance between topographic forcing and background flow, where the Coriolis effect and topographic steering collectively maintain directional propagation stability.

The terrain-modulated wave behavior observed here—including stable contour translation and asymmetric inner-region distributions—establishes a baseline for investigating multifactor coupling effects. Subsequent studies may extend this framework by incorporating thermal forcing into the shallow-water system, thereby exploring synergistic terrain–thermal regulation of wave trajectories. Such expansions would advance the dynamics of Rossby waves in complex environments, whereas the present study remains focused on quantifying topographic modulation in isolation.

4. Conclusions

This study investigates topographic Rossby algebraic solitary waves (TRASWs) in mid-to-high-latitude geophysical fluids, with the aim of establishing a theoretical model for their amplitude evolution. Starting from the shallow-water equations governing rotating fluid motion, the model incorporates the shallow-water approximation, β-plane approximation, and weak nonlinear perturbation methods. Through nondimensionalization and matching of inner and outer regional solutions, a dimensionless BDO equation is derived. This equation includes a nonlinear amplitude term, a linear phase speed term, and a Hilbert transform dispersion term, providing a quantitative description of the topographic modulation of TRASW amplitude and filling a theoretical gap in the modeling of algebraic solitary waves under weak to moderate topographic conditions.

The study employs a Physics-Informed Neural Network for validation. The PINN simulation results show a relative error of only 3.58×10^{-2} compared to the theoretical solution, effectively avoiding numerical dispersion issues associated with traditional methods and confirming the validity of the BDO-type equation.

However, the study has certain limitations: the quantitative influence of topographic parameters on wave amplitude remains inadequately characterized, and wave speed calculations have not been addressed. Future work will focus on optimizing topographic parameterization, quantitatively evaluating the effects of topography on wave amplitude and speed, and incorporating temporal variations in background flow fields to further refine the dynamical theory of TRASWs.

Author Contributions: Methodology, W.Z., Q.L., L.Y. and R.Z.; Investigation, W.Z., Q.L., L.Y. and R.Z.; Writing—original draft, W.Z.; Writing—review & editing, W.Z.; Supervision, R.Z.; Funding acquisition, Q.L., L.Y. and R.Z. All authors have read and agreed to the published version of the manuscript.

Funding: This work is supported by the National Natural Science Foundation of China (Nos. 12462021, 12102205 and 12262025), the Central Guidance for Local Scientific and Technological Development Funding Projects (2024ZY0117), the Outstanding Youth Science Fund Project of the Natural Science Foundation of Inner Mongolia Autonomous Region (2025JQ006), the Program for Talent Revitalization of Inner Mongolia Team (2025TEL06), the Program for Young Talents of Science and Technology in Universities of Inner Mongolia Autonomous Region (NJYT23098), the Scientific Starting and the Innovative Research Team in the Universities of Inner Mongolia Autonomous Region of China (NMGIRT2208), the National Natural Science Foundation of Inner Mongolia Autonomous Region (2025QN01014).

Institutional Review Board Statement: Not applicable.

Informed Consent Statement: Not applicable.

Data Availability Statement: The original contributions presented in this study are included in the article. Further inquiries can be directed to the corresponding author.

Conflicts of Interest: The authors declare no conflicts of interest.

Appendix A

The following expressions are parameters of Equation (36):

$$\sigma = \int_{-L}^{L} \frac{\overline{\beta}(y)}{(\overline{U}-c_0)^2}\phi^2(y)\mathrm{d}y \qquad D = \frac{1}{\sigma}[\phi(L)-\phi(-L)]$$

$$S = \frac{1}{\sigma}[\phi^2(L)+\phi^2(-L)] \qquad Q = \frac{1}{\sigma}\int_{-L}^{L}\frac{\phi^3(y)}{\overline{U}-c_0}\frac{\mathrm{d}}{\mathrm{d}y}\left(\frac{\overline{\beta}(y)}{\overline{U}-c_0}\right)\mathrm{d}y$$

$$F = \frac{1}{\sigma}\delta\int_{-L}^{L}\Omega(y)\frac{\overline{\beta}(y)}{\overline{U}-c_0}\phi^2(y)\mathrm{d}y \qquad M = \frac{3}{\sigma}\delta\int_{-L}^{L}\overline{U}'\frac{\phi^2(y)}{\overline{U}-c_0}\Omega'(y)\mathrm{d}y$$

$$V = \frac{1}{\sigma}\int_{-L}^{L}\frac{\phi^2(y)}{\overline{U}-c_0}\Omega'(y)\mathrm{d}y \qquad G = \frac{1}{\sigma}\delta\int_{-L}^{L}\phi^2(y)\Omega''(y)\mathrm{d}y$$

$$E = \frac{1}{\sigma}\delta\int_{-L}^{L}\phi(y)\frac{\partial\phi}{\partial y}\Omega'(y)\mathrm{d}y \qquad Z = \frac{1}{\sigma}\delta\int_{-L}^{L}\Omega(y)\frac{\phi^2(y)}{\overline{U}-c_0}\frac{\mathrm{d}^2\overline{U}}{\mathrm{d}y^2}\mathrm{d}y.$$

References

1. Rossby, C.G. Relation between variations in the intensity of the zonal circulation of the atmosphere and the displacements of the semi-permanent centers of action. *J. Mar. Res.* **1939**, *2*, 38–55. [CrossRef]
2. Hoskins, B.I.; Karoly, D.J. The steady linear response of a spherical atmosphere to thermal and orographic forcing. *J. Atmos. Sci.* **1981**, *38*, 1179–1196. [CrossRef]
3. Rhines, P.B. Waves and turbulence on a beta-plane. *J. Fluid Mech.* **1975**, *69*, 417–443. [CrossRef]
4. Long, R.R. Solitary waves in the westerlies. *J. Atmos. Sci.* **1964**, *21*, 197–200. [CrossRef]
5. Benney, D.J. Long nonlinear waves in fluid flow. *J. Math. Phys.* **1966**, *45*, 52–63. [CrossRef]
6. Larsen, L.N. Comments on: Solitary waves in the Westerlies. *J. Atmos. Sci.* **1965**, *22*, 222–224. [CrossRef]
7. Clarke, R.A. Solitary and cnoidal planetary waves. *Geophys. Fluid Dyn.* **1971**, *2*, 343–354. [CrossRef]
8. Woollings, T.; Li, C.; Drouard, M. The role of Rossby waves in polar weather and climate. *Weather Clim. Dyn.* **2023**, *4*, 61–80. [CrossRef]
9. Charney, J.G.; DeVore, J.G. Multiple flow equilibria in the atmosphere and blocking. *J. Atmos. Sci.* **1979**, *36*, 1205–1216. [CrossRef]
10. Zhang, Z.H.; Zhang, R.G.; Wang, J.; Yang, L.G. Dynamics of Rossby wave packets with topographic features via derivative expansion approach. *Nonlinear Dyn.* **2023**, *111*, 17483–17497. [CrossRef]
11. Yang, H.W.; Xu, Z.H.; Yang, D.Z. ZK-Burgers equation for three-dimensional Rossby solitary waves and its solutions as well as chirp effect. *Adv. Differ. Equ.* **2016**, *2016*, 167 . [CrossRef]
12. Yang, H.W.; Chen, X.; Guo, M. A new ZKCBO equation for three-dimensional algebraic Rossby solitary waves and its solution as well as fission property. *Nonlinear Dyn.* **2018**, *91*, 2019–2032. [CrossRef]
13. Abernathey, R.; Marshall, J.; Ferreira, D. The dependence of Southern Ocean meridional overturning on wind stress. *J. Phys. Oceanogr.* **2011**, *41*, 2261–2278. [CrossRef]
14. Abernathey, R.; Cessi, P. Topographic enhancement of eddy efficiency in baroclinic equilibration. *J. Phys. Oceanogr.* **2014**, *44*, 2107–2126. [CrossRef]
15. Zhao, B.J.; Wang, J.X. Forced solitary wave and vorticity with topography effect in quasi-geostrophic modelling. *Adv. Mech. Eng.* **2023**, *15*, 1–10. [CrossRef]
16. Chen, C.; Kamenkovich, I. Effects of topography on Baroclinic instability. *J. Phys. Oceanogr.* **2013**, *43*, 790–804. [CrossRef]
17. Yu, Z.Y.; Hao, Z.J.; Xu, Z.H.; Zhang, P.; Yin, B.S.; Yang, H.W. Satellite observations of coastal upwelling in the northern arafura sea. *J. Oceanogr. Limnol.* **2024**, *42*, 361–376. [CrossRef]
18. Yang, H.W.; Zhang, Z.C.; Shu, J.; Han, Y. Gradient nanostructure, enhanced surface integrity and fatigue resistance of Ti-6Al-7Nb alloy processed by surface mechanical attrition treatment. *Mater. Sci. Technol.* **2024**, *188*, 252–269. [CrossRef]
19. Zhao, J.; Yang, H.W. Backdoor two-stream video models on federated learning. *ACM Trans. Multim. Comput. Commun. Appl.* **2024**, *20*, 1–20. [CrossRef]
20. Yang, H.W.; Yang, D.Z.; Shi, Y.L.; Jin, S.S.; Yin, B.S. Interaction of algebraic rossby solitary waves with topography and atmospheric blocking. *Dyn. Atmos. Oceans* **2015**, *71*, 21–34. [CrossRef]
21. Vanneste, J. Rossby wave frequency change induced by small-scale topography. *J. Phys. Oceanogr.* **2000**, *30*, 1820–1826. [CrossRef]
22. Han, F.Y.; Liu, Q.S.; Yin, X.J.; Zhang, R.G. On the dynamics of Rossby algebraic solitary waves induced by large-scale topography. *Phys. Fluids* **2024**, *36*, 1000. [CrossRef]
23. Zhang, Z.H.; Zhang, R.G.; Yang, L.G.; Liu, Q.S. On the dynamics of nonlinear Rossby solitary waves via the Ostrovsky hierarchy. *Phys. Fluids* **2024**, *36*, 076614. [CrossRef]

24. Hou, S.T.; Zhang, R.G.; Zhang, Z.H.; Yang, L.G. On the Quartic Korteweg-de Vries hierarchy of nonlinear Rossby waves and its dynamics. *Wave Motion* **2024**, *124*, 103249. [CrossRef]
25. Wang, J.; Zhang, R.G.; Yang, L.G. Solitary waves of nonlinear barotropic-baroclinic coherent structures. *Phys. Fluids* **2020**, *32*, 096604. [CrossRef]
26. Wang, J.; Zhang, R.G.; Yang, L.G.; Liu, Q.S. On the dynamics of nonlinear barotropic-baroclinic interactions through a coupled Gardner hierarchies approach. *Phys. Fluids* **2023**, *35*, 086603. [CrossRef]
27. Gao, S.T. Nonlinear rossby wave induced by large-scale topography. *Adv. Atmos. Sci.* **1988**, *5*, 301–310.
28. Benilov, E.S. Baroclinic instability of two-layer flows over one-dimensional bottom topography. *J. Phys. Oceanogr.* **2001**, *31*, 2019–2025. [CrossRef]
29. Uchimoto, K.; Kubokawa, A. Form drag caused by topographically forced waves in a barotropic β channel: Effect of higher mode resonance. *J. Oceanogr.* **2005**, *61*, 197–211. [CrossRef]
30. Zhang, J.Q.; Zhang, R.G.; Yang, L.G.; Liu, Q.S.; Chen, L.G. Coherent structures of nonlinear barotropic-baroclinic interaction in unequal depth two-layer model. *Appl. Math. Comput.* **2021**, *408*, 126347. [CrossRef]
31. Song, J.; Liu, Q.S.; Yang, L.G. Beta effect and slowly changing topography rossby waves in a shear flow. *Acta Phys. Sin.* **2012**, *61*, 210510. [CrossRef]
32. Meng, L.; LÜ, K.L. Influences of dissipation on interaction of solitary wave with localized topography. *Chin. J. Comput. Phys.* **2002**, *19*, 349–356.
33. Debnath, L. On linear and nonlinear Rossby waves in an ocean. *J. Math. Anal. Appl.* **2007**, *333*, 164–190. [CrossRef]
34. Yan, Z. An improved algebra method and its applications in nonlinear wave equations. *Chaos Solitons Fractals* **2004**, *21*, 1013–1021. [CrossRef]
35. Wooyoung, C.; Camassa, R. Fully nonlinear internal waves in a two-fluid system. *J. Fluid Mech.* **1999**, *396*, 1–36. [CrossRef]
36. Yuan, C.; Grimshaw, R.; Johnson, E. The propagation of internal solitary waves over variable topography in a horizontally two-dimensional framework. *J. Phys. Oceanogr.* **2018**, *48*, 283–300. [CrossRef]
37. Craig, W.; Guyenne, P.; Sulem, C. Water waves over a random bottom. *J. Fluid Mech.* **2009**, *640*, 79–107. [CrossRef]
38. Scaife, A.A.; Comer, R.E.; Dunstone, N.J.; Knight, J.R.; Smith, D.M.; MacLachlan, C.; Martin, N.; Peterson, K.A.; Rowlands, D.; Carroll, E.B.; et al. Corrigendum to: Tropical rainfall, Rossby waves and regional winter climate predictions. *Q. J. R. Meteorol. Soc.* **2019**, *145*, 1307. [CrossRef]
39. Nakamoto, S.; Liu, J. Solitonlike solutions from the potential vorticity equation over topography. *J. Geophys. Res. Oceans* **1991**, *96*, 7077–7081. [CrossRef]
40. Klimachkov, D.A.; Petrosyan, A.S. Rossby waves in the magnetic fluid dynamics of a rotating plasma in the shallow-water approximation. *J. Exp. Theor. Phys.* **2017**, *125*, 597–612. [CrossRef]
41. Liu, Y.; Varlamov, V. Stability of solitary waves and weak rotation limit for the Ostrovsky equation. *J. Differ. Equ.* **2004**, *203*, 159–183. [CrossRef]
42. Laughman, B.; Fritts, D.C. Comparisons of predicted bore evolutions by the Benjamin-Davis-Ono and Navier-Stokes equations for idealized mesopause thermal ducts. *J. Geophys. Res. Atmos.* **2011**, *116*, D02120. [CrossRef]
43. Fournier, A. Wavelet representation of lower-atmospheric long nonlinear wave dynamics, governed by the Benjamin-Davis-Ono-Burgers equation. *Wavelet Appl.* **1995**, *2491*, 672–681.
44. Flamarion, M.V.; Pelinovsky, E. Irregular dynamics of internal waves in a weakly stratified fluid in the viscous Benjamin-Ono equation model. *Theor. Math. Phys.* **2025**, *224*, 1126–1135. [CrossRef]
45. Raissi, M.; Perdikaris, P. Physics-informed neural networks: A deep learning framework for solving forward and inverse problems involving nonlinear partial differential equations. *J. Comput. Phys.* **2019**, *378*, 686–707. [CrossRef]
46. Zhao, M.; Qu, C. Classification of the two-component Benjamin-Ono systems. *Theor. Math. Phys.* **2024**, *219*, 638–662. [CrossRef]
47. Ono, H. Algebraic solitary waves in stratified fluids. *J. Phys. Soc. Jpn.* **1975**, *39*, 1082–1091. [CrossRef]
48. Ono, H. Algebraic Rossby Wave Soliton. *J. Phys. Soc. Jpn.* **1981**, *50*, 3833. [CrossRef]

Disclaimer/Publisher's Note: The statements, opinions and data contained in all publications are solely those of the individual author(s) and contributor(s) and not of MDPI and/or the editor(s). MDPI and/or the editor(s) disclaim responsibility for any injury to people or property resulting from any ideas, methods, instructions or products referred to in the content.